STM JOURNALS

Journal of
Offshore Structure and Technology

ISSN: 2349-8986
Volume 11, Issue 3, 2024
September–December
DOI (Journal): 10.37591/JoOST

https://journals.stmjournals.com/joost

Research JoOST

Vibrational Wind Turbine Design

Carlos Armenta-Déu[1,*], Ignacio Madrazo[2],
Jorge Contreras[3], Matilde Santos[4]

Abstract

This work focuses on the study and analysis of bladeless wind turbines (BWT) as an alternative to operating vertical-axis wind turbines (VAWT) and horizontal-axis wind turbines (HAWT). A mathematical analysis of the BWT oscillation under wind force allows the development of specific mathematical expressions for the oscillation speed and BWT mast displacement at any height. The oscillation movement is submitted to a Strouhal constant number condition, resulting in an algorithm that allows the determination of the BWT mast profile to maintain a constant vortex shedding oscillation frequency, a required condition to preserve the integrity of the mast material and to reduce fatigue and mechanical stress. The predicted results from the mathematical analysis show a good agreement, higher than 95% on average, with reported data in literature, thus, validating the proposed mathematical procedure. A simulation run for a designed prototype shows a high agreement between mathematical development and the linear approach currently adopted by the manufacturing processes (R^2=0.9885); therefore, the proposed methodology for the BWT design is valid.

Keywords: Wind energy, bladeless wind turbine, performance simulation and optimization, turbulent wind regime operation, vortex

INTRODUCTION

World energy consumption continues to increase as the population grows, and countries evolve to a higher standard of living [1–3]. The power generation source to support energy demand resides in fossil fuels, which will persist for decades, following expert opinions [4–7]. In the past decade (2010–2020), the renewable energy sector grew from 12.3% to 16.8%, whereas the non-renewable energy sector decreased from 87.7% to 83.2%, indicating a high global dependence on fossil fuel resources [8]. Renewable energy is a feasible alternative to fossil fuels, particularly solar and wind energy, although the power coverage factor for electricity generation remains below 50% in many countries [9–12]. Figure 1 shows the rapid solar photovoltaic growth and persistent increase in wind energy compared to the stagnated development of alternative renewable energy sources. The slow-growing rate of renewable energies in the world electricity generation sector, barely 0.45% per year, forces us to encourage the implementation of alternative power sources to replace fossil fuels [13–15]. To this end, authorities and organizations promote the implementation of renewable energy installations through regulations to make people react to the reluctance to change from conventional power systems to renewable ones. Additionally, incentives and subsidies help support investment in implementing renewable systems, especially solar photovoltaic arrays and wind turbines [16–19].

***Author for Correspondence**
Carlos Armenta-Déu
E-mail: cardeu@fis.ucm.es

[1,3]Professor, Department of Matter Structure, Thermal Physics and Electronics, Faculty of Physical Sciences, Complutense University of Madrid, 28040 Madrid, Spain
[2]Student (Postgraduate), Department of Matter Structure, Thermal Physics and Electronics, Faculty of Physical Sciences, Complutense University of Madrid, 28040 Madrid, Spain
[4]Professor, Department of Computer Architecture and Automatic Control, Faculty of Computer Science, Complutense University of Madrid, 28040 Madrid, Spain

Received Date: September 10, 2024
Accepted Date: October 04, 2024
Published Date: October 07, 2024

Citation: Carlos Armenta-Déu, Ignacio Madrazo, Jorge Contreras, Matilde Santos. Vibrational Wind Turbine Design. Journal of Offshore Structure and Technology. 2024; 11(3): 32–45p.

Wind Energy State of the Art

Wind energy experiments are relevant to the development of wind offshore technology and the implementation of marine wind farms owing to higher wind turbines and access to open spaces with no natural obstacles or restrictions owing to human settlements [20–25].

Offshore wind farms represent a solution to the limited land available for onshore wind power plants. The orography and wind turbine rotors generate turbulence that reduces the efficiency of conventional three-blade horizontal-axis wind turbines, forcing wind farm designers to increase the distance between adjacent wind turbines, which reduces the available space and chances of building new wind farms [26–28].

Although offshore wind farms, such as inland wind power plants, do not suffer from turbulent winds, a minimum distance should be maintained to avoid the influence of wakes on the performance of adjacent turbines [29–32].

An alternative to the wake problem is to implement a new wind turbine model with good performance under turbulent winds [33–35]. We propose a bladeless wind turbine (BWT) that uses turbulent wind as a power source to produce mechanical energy for electricity generation. A BWT can be installed offshore in free space between giant marine wind turbines [36]. To date, BWT operates in small prototypes [37] (Figure 2), using turbulent wind as a driving force to vibrate and generate kinetic energy that is converted into electricity.

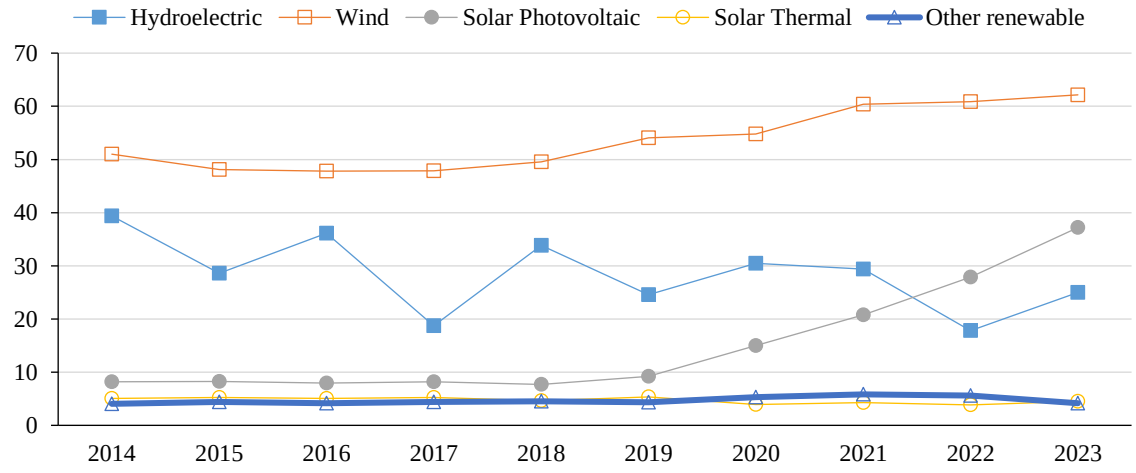

Figure 1. Renewable energy sources evolution.

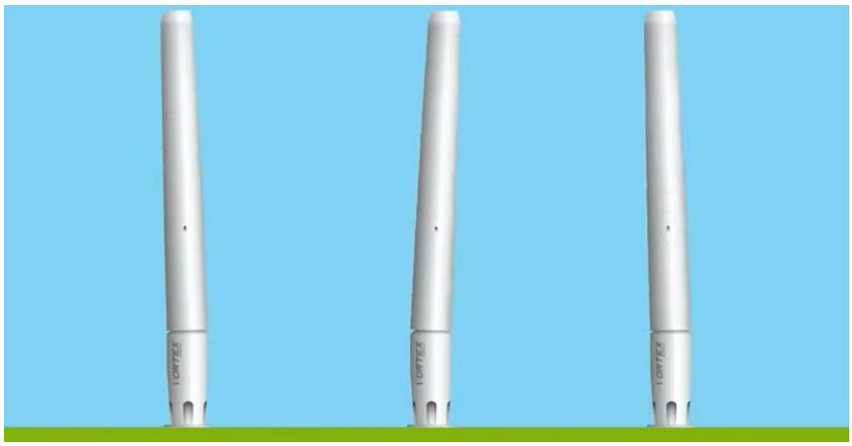

Figure 2. View of a bladeless wind turbine (BWT).

Implementing BWT in the offshore wind farm free space has two advantages: first, extra power generation, and second, lowering the wake power, limiting the influence on the next conventional wind turbine, and allowing a distance reduction between two consecutive turbines. Therefore, this configuration results in a higher global offshore wind farm performance. Additional advantages of the BWT are its design simplicity, low maintenance, low sound level, and minimal environmental impact, especially for birds. In addition, owing to its symmetric design, a BWT uses all-directional winds, eliminating the yaw mechanism and optimizing the performance.

THEORETICAL FOUNDATIONS

Aerodynamic Force on BWT

The wind force striking the BWT structure decomposes into two fractions: drag force, which is responsible for the momentum transmission to the aerodynamic body in a front collision, and lift force, perpendicular to the wind direction, which creates a rotation effect on the collided surface. The drag force depends on many factors, such as the blade geometry, type of material, and rugosity, making it difficult to determine its value. Therefore, the classical method of expressing the drag force is through the drag coefficient, C_D, using the equation:

$$F_D = \frac{1}{2}\rho C_D A u^2 \tag{1}$$

ρ and u are the air density and speed, respectively, and A is the wind rotor blade section.

Term $(1/2)\rho A u^2$ represents the dynamic wind force. The drag coefficient was empirically determined.

The lift force is derived from Bernoulli's principle; indeed, in a blade with non-symmetric geometry, the wind moves faster along the longest blade side; therefore, applying Bernoulli's principle to such geometry (Figure 3), we have

A bladeless wind turbine resembles a round cylinder, where the wind never strikes asymmetrically as long as a laminar flow exists. When the drag forces predominate, for Reynolds numbers above 4000 [38], a pressure difference appears on both sides of the cylinder, generating a pressure movement crosswise to the wind and creating a lift force.

The lift force is also complex to determine; therefore, we apply the same procedure as for the drag force, using the lift coefficient C_L and the dynamic wind force through the expression [39].

$$F_L = \frac{1}{2}\rho C_L A u^2 \tag{2}$$

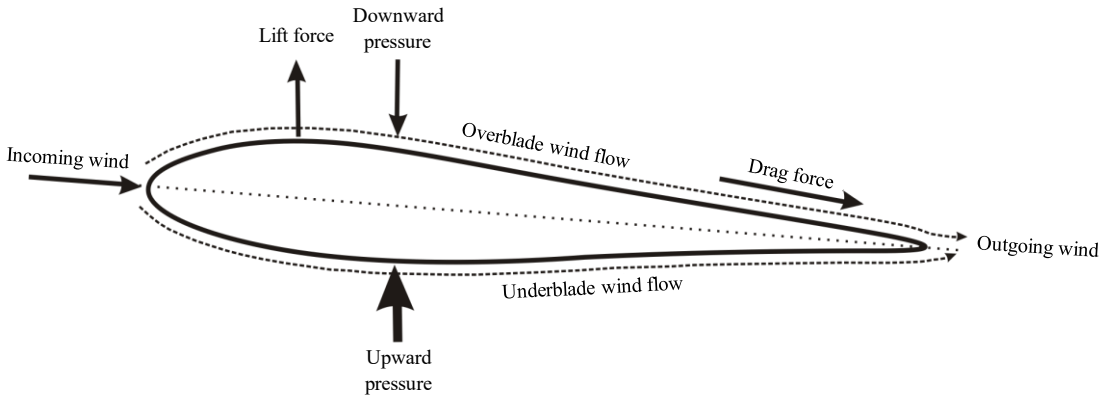

Figure 3. Schematic view of the wind force decomposition.

Owing to the crosswise movement, the cylinder compresses the air in the direction of movement, expanding the air in the opposite direction, generating a pressure gradient opposite to the one that initiates the movement and creates an oscillation [40]. This type of oscillation is known as *vortex-induced vibrations (VIV)*, an aerodynamic phenomenon characterized by symmetric vortex wakes periodically emitted from the cylinder in the incoming wind direction and von Karman vortices.

The vortex frequency depends on the wind speed, cylinder diameter, and Strouhal number (St) as follows [37].

$$f_u = \frac{St \cdot u}{D} \tag{3}$$

The process through which the vortices come off from the cylinder surface is known as *vortex shedding* and is responsible for lift force generation. The eddy release causes cylinder oscillation whose frequency matches that of the vortex [41]. The emitted wake type is shown in Figure 4 as a function of the wind speed and Reynolds number.

The vortex frequency calculation requires determination of the Strouhal number because the cylinder diameter and wind speed are easy to measure. The Strouhal number is related to the Reynolds and Roshko numbers (Ro) by the following equation:

$$St = Ro/\mathrm{Re} \tag{4}$$

Where the Roshko number depends on the Reynolds number as:

$$Ro = \begin{cases} 0.212\,\mathrm{Re} - 4.5 \rightarrow 50 < \mathrm{Re} < 200 \\ 0.212\,\mathrm{Re} - 2.7 \rightarrow 200 < \mathrm{Re} < 2000 \end{cases} \tag{5}$$

Above Re=2000, the Roshko number moves in the range of Ro=0.20±0.02 for $2000<\mathrm{Re}<10^6$; therefore, for turbulent flow with a Reynolds number above 2000, we consider the Roshko number constant and equal to 0.21.

	No separation. Creeping flow	Re < 5
	A fixed pair of symmetric vortices	5 < Re < 40
	Laminar vortex street	40 < Re < 300
	Transition to turbulence in the wake	200 < Re < 300
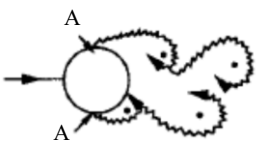	Wake completely turbulent. A: Laminar boundary layer separation	$300 < \mathrm{Re} < 3\times10^5$ Subcritical

Figure 4. BWT wake type generation as a function of Reynolds number.

WIND TURBINE STRUCTURE

The wind turbine design comprises an oscillating rigid cylinder mast and flexible stand connected to the device base [41]. Because the vortex frequency depends on the wind speed and mast diameter, these two factors are critical in wind turbine design. Because the wind direction is variable, the mast should be symmetric with respect to the vertical axis but not necessarily cylindrical; a truncated cone geometry is also valid. This last configuration solves the problem of an increasing mast section with height because of the need for higher mechanical resistance with height owing to the higher wind dynamic force. Indeed, the wind speed increases with height following a potential law; therefore, the dynamic forces increase with the square power of the speed, forcing the mast to have higher mechanical resistance as we move upward.

By retrieving Equation (3), we notice that the mast diameter should increase with wind speed, keeping the ratio u/D constant to maintain a constant frequency along the mast. If the frequency changes from one mast section to another, the mast suffers from crosswise mechanical forces, which may damage the wind turbine structure and eventually produce mast breakage. Figure 5 shows a symbolic representation of the wind forces acting on the wind turbine structure for different mast sections. We observe that, for a cylindrical mast, the wind forces increase as the height increases, whereas for the truncated cone configuration, the forces are identical at all mast sections.

BWT WIND FARM LAYOUT

The BWT also produces turbulent wakes, forcing the separation of two adjacent turbines at a minimum distance. If they are too close, the *Wake Galloping* effect appears (Figure 6). The Wake Galloping effect is based on the following mechanism: the wind stream interacts with the first turbine and produces downwind vortices, and the wakes induce crosswise lift forces on the next turbine, as indicated by the red arrow in Figure 6, creating a reinforced periodic oscillatory movement.

The energy associated with the Wake Galloping effect is high and may affect the wind turbine structure, causing damage and even breakage. Therefore, they should be avoided. The Vortex Company considers that the minimum distance between the turbines to attenuate the Wake Galloping effect should match half the turbine height [40]. Figure 7 shows the CFD simulation of the Wake Galloping mechanism.

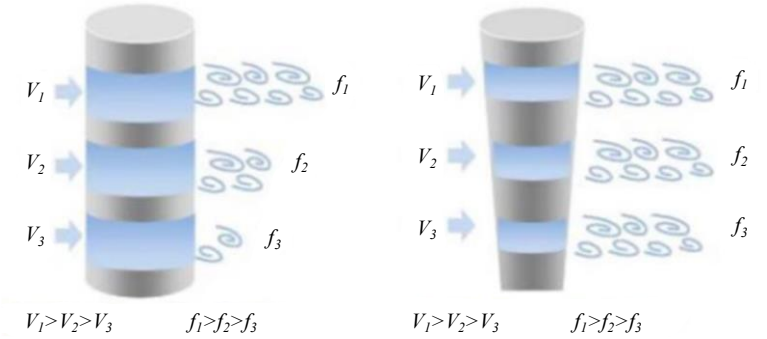

Figure 5. Symbolic representation of the wind forces on the BWT structure.

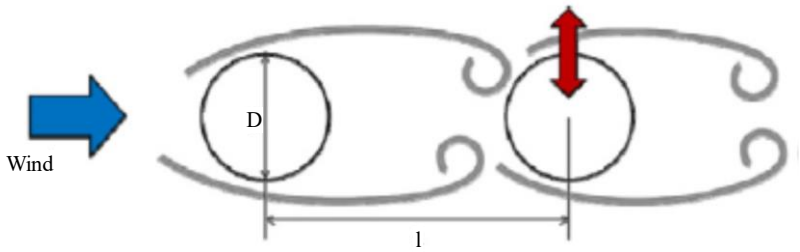

Figure 6. Wake galloping effect.

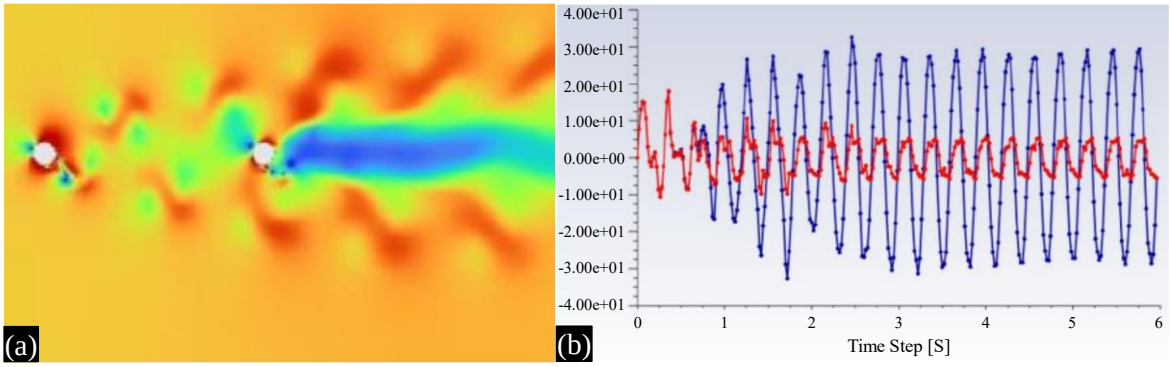

Figure 7. Wake galloping mechanism simulation using CFD technique: (a) wake galloping phenomenon; (b) wind turbine lift coefficient [41]

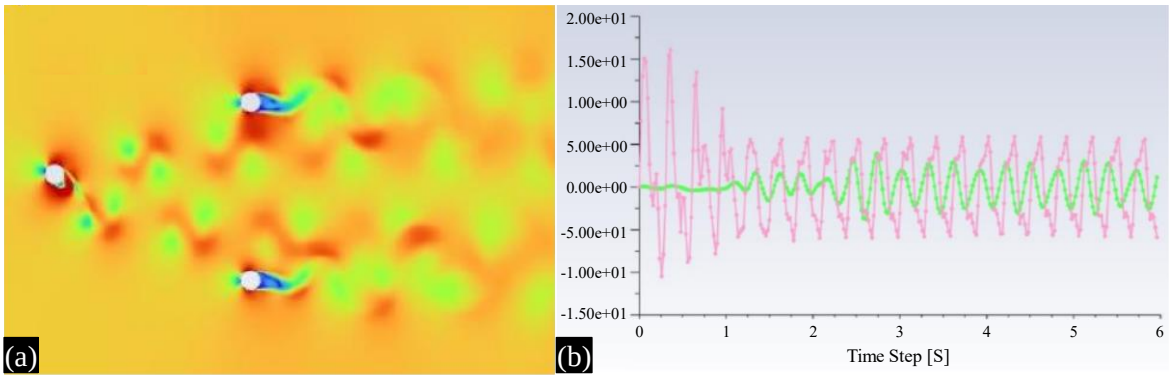

Figure 8. Reduction of the Wake Galloping mechanism using a triangle configuration: (a) wake galloping simulation using CFD technique: (b) wind turbine lift coefficient.

We observe how the turbulent wakes rise in amplitude as they move away from the turbine (left hand of Figure 7). We also notice that the second turbine lift coefficient (blue line) is considerably higher than that of the first turbine (red line), indicating that the wind force intensity and mechanical stress increase (right-hand side).

Mechanical stress is relevant because it causes cumulative damage to the mast structure; when the cumulative damage reaches the threshold value, the structure collapses, and the mast breaks. A proposed solution to avoid the Wake Galloping effect is to configure the BWT layout as a triangle; this configuration considerably reduces the Wake Galloping mechanism (Figure 8).

The left side of Figure 8 shows how the turbulence disperses in the new configuration, thereby reducing the wake effects generated by BWT. On the other hand, the lift coefficient of the downwind BWT was lower (green line), indicating a reduced intensity of the turbulent wake. Therefore, we can install more than one BWT behind the first one with minimal effects and low mechanical stress.

MATHEMATICAL ANALYSIS

The oscillatory movement mathematical analysis in the BWT evaluates the mast displacement in the X-Y plane when subjected to a wind force. Because the BWT comprises a rigid mast and flexible stand, we divided the structure into two parts, each corresponding to the mast and stand sections (Figure 9).

L and *H* are the stands and total BWT height, respectively. *D* is the mast diameter. We considered a truncated cone geometry to maintain a constant frequency throughout the structure.

The condition applying for the Strouhal Equation (3) requires a null rod displacement. Under such conditions, only the wind speed is considered. The first step is to determine the height that fulfills this condition.

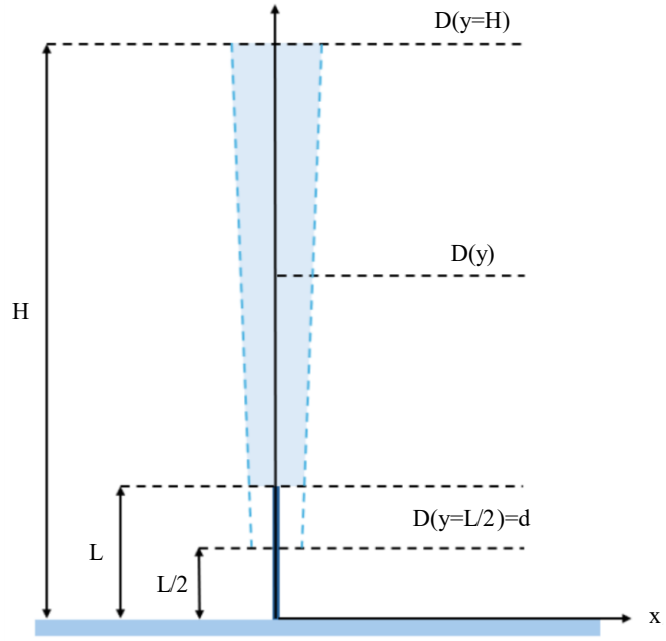

Figure 9. Schematic representation of the BWT.

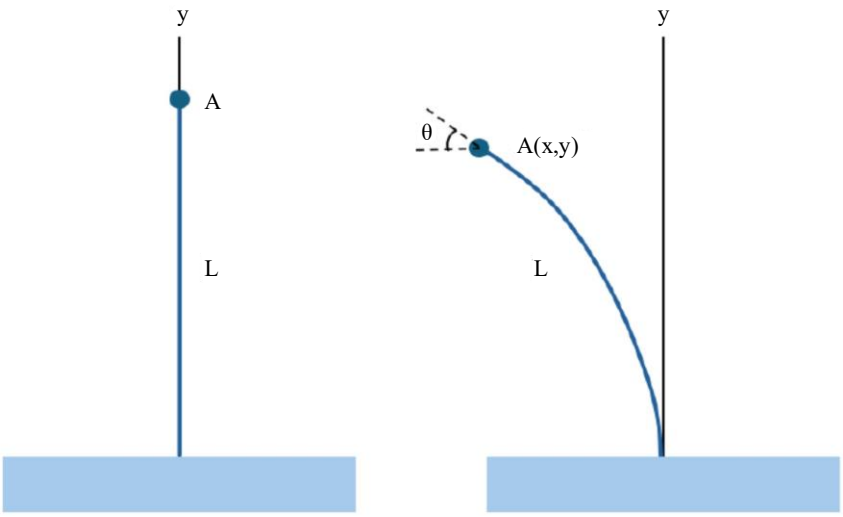

Figure 10. BWT mast bending movement.

We started considering the BWT mast as a cantilever beam with one end anchored to the ground and the opposite end free to move and subjected to a force that bends the mast with the free-end describing a circular path (Figure 10).

The free-end position corresponds to a point of the circular path; therefore:

$$R^2 = (x - R)^2 + y^2 \tag{6}$$

x and *y* are the Cartesian coordinates of the free-end position (Figure 11).

Because the mast length is constant:

$$L = R\theta \tag{7}$$

Where Θ is the flexion angle.

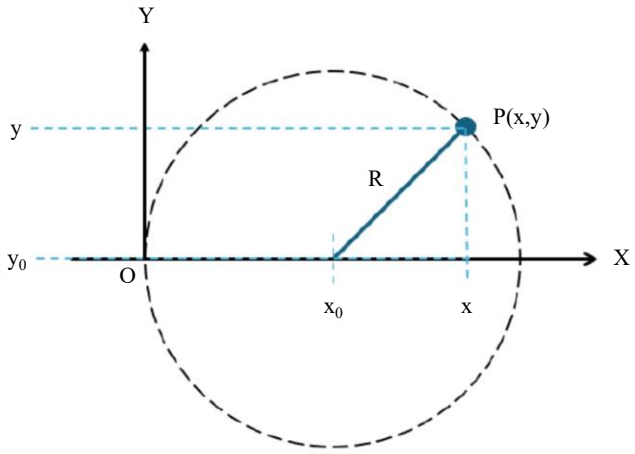

Figure 11. Graph representation of the free-end positioning.

Combining Equations (6) and (7):

$$\left(\frac{L}{\theta}\right)^2 = \left(x - \frac{L}{\theta}\right)^2 + y^2 \rightarrow x^2 - 2x\frac{L}{\theta} + y^2 = 0 \tag{8}$$

On the other hand, from Figure 10:

$$R = \frac{y}{\sin\theta}\,;\, x = y\frac{1-\cos\theta}{\sin\theta} \tag{9}$$

Combining Equations (7) to (9):

$$x = \frac{2L}{\theta\left[1+\dfrac{\sin^2\theta}{(1-\cos\theta)^2}\right]}\,;\, y = \frac{2L\sin\theta}{\theta\left[1+\dfrac{\sin^2\theta}{(1-\cos\theta)^2}\right](1-\cos\theta)} \tag{10}$$

Equation (10) shows the cantilever beam-free-end coordinates. The vibration mode can be determined using Equation (7) because it calculates the curvature radius for every flexion angle. Figure 12 shows the cantilever free-beam displacement evolution with a variable flexion angle for a 2 m-long mast.

Literature shows that the height at which the oscillation is negligible corresponds to half of the mast length [42]. Applying the data from our calculation to a height of L/2, we obtained (Table 1). We observe that the maximum D/L ratio is 0.065, which is negligible according to the literature specifications. Therefore, we can validate our calculation procedure.

MAST DESIGN AND CALCULATION OF VORTEX SHEDDING FREQUENCY

If we apply the Strouhal number to our system, we obtain:

$$f\left(\frac{L}{2}\right) = \frac{St(L/2)v_r}{d} \tag{11}$$

With d=D for y=L/2. V_r represents the relative speed between the wind and mast.

Equation (11) shows the vortex shedding frequency at the height at which oscillation is negligible. In mathematical development, we assume that this frequency should be constant at any height.

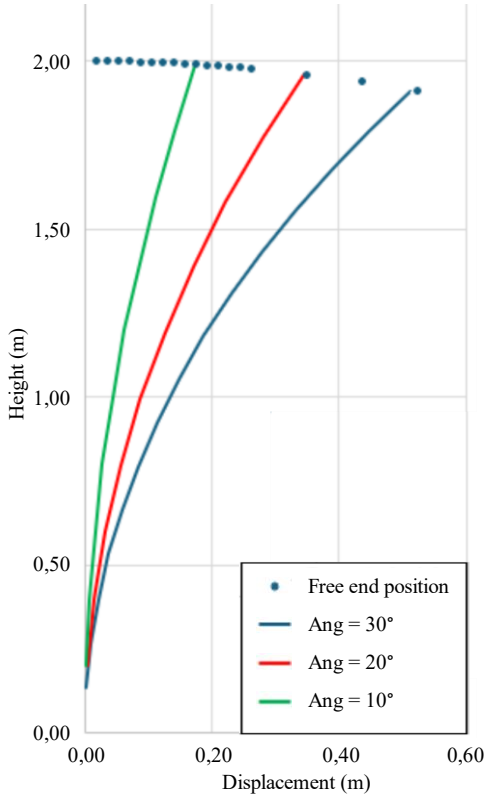

Figure 12. Evolution of the mast free-end with flexion angle.

Table 1. Displacement (D) of the mast position at L/2 for variable flexion angles.

Angle (°)	D (m)	D/L (%)
10	0.05	2.5
20	0.09	4.5
30	0.13	6.5

Since wind and mast movement direction are perpendicular, the relative speed is:

$$v_r = \left(v_w^2 + v_{osc}^2\right)^{1/2} \tag{12}$$

v_w and v_{osc} are the wind and mast oscillation speeds.

However, the wind speed evolves with height according to the exponential law [43]

$$v(y) = v_o \left(\frac{y}{y_o}\right)^{\alpha} \tag{13}$$

For neutral stability conditions, $\alpha=1/7$ [44]; however, if atmospheric conditions evolve, the α-coefficient differs [45].

Since we can express the oscillation speed as:

$$v_{osc} = \frac{4A}{T} = 4X(y)f \tag{14}$$

A, *T*, and *f* are the oscillation amplitude, period, and frequency, respectively, and X(y) is the displacement at the y height.

Combining Equations (12) to (14), we have:

$$v_r = \left\{ \left[v_o \left(\frac{y}{y_o} \right)^{\alpha} \right]^{1/2} + 16 X^2(y) f^2 \right\}^{1/2} \tag{15}$$

And relating Equation (3) and (15):

$$f(y) = \left\{ \frac{(St)^2 \left[v(y) \right]^2}{\left[D(y) \right]^2 - 16(St)^2 \left[X(y) \right]^2} \right\}^{1/2} \tag{16}$$

Where:

$$D(y) = \left\{ \frac{\left[v(y) \right]^2}{\left[v\left(\frac{L}{2} \right) \right]^2} d^2 + 16(St)^2 \left[X(y) \right]^2 \right\}^{1/2} \tag{17}$$

We define the *D(y)* dependence on height through the variable β defined as:

$$\beta = \frac{X(H)}{D(H)} \tag{18}$$

H is the mast height-free-end.

The oscillation amplitude at any height is:

$$X(y) = \frac{y - L/2}{H - L/2} \beta D(H) \tag{19}$$

Combining Equations (17) and (18) and operating:

$$D(H) = \left\{ \frac{\left[v(H) \right]^2 d^2}{\left[v\left(\frac{L}{2} \right) \right]^2 \left[1 - 16\beta^2 (St)^2 \right]} \right\}^{1/2} \tag{20}$$

Now, replacing in Equation (19):

$$D(y) = \left\{ \frac{d^2}{\left[v\left(\frac{L}{2} \right) \right]^2} \left[\left[v(y) \right]^2 + \frac{16\beta^2 (St)^2 \left[v(H) \right]^2}{1 - 16\beta^2 (St)^2} \left(\frac{y - L/2}{H - L/2} \right)^2 \right] \right\}^{1/2} \tag{21}$$

A similar mathematical development was derived from the Vortex Company Patent [46], proving the validity of our procedure.

SIMULATION

We consider a BWT with a base length of 2 m, a diameter of 0.18 m, and a total mast height of 6 m. The wind profile showed a speed of 12 m/s at a height of 10 m. The terrain rugosity coefficient is 0.18. By applying Equation (20) and considering β=1, we can determine the oscillation amplitude at any height using Equation (19). From Equation (3), for a height y=L/2, we obtain the vortex shedding frequency, which is considered constant for all mast lengths. Therefore, using this frequency and the oscillation amplitude at any height, given by Equation (14), we can determine the oscillation speed at any height. Once we calculate the wind and oscillation speed, we can determine the relative speed between the mast and the wind by applying Equation (12). Finally, we used Equation (21) to determine the mast diameter at any height to maintain a constant vortex shedding frequency. Table 2 lists the results for heights between 1 and 6 m. Figure 13 shows the BWT mast design. The blue line corresponds to mathematical development, whereas the red line corresponds to manufacturing approximation.

Table 2. Oscillation speed and mast diameter for heights between 1 and 6 m.

h (m)	v_w (m/s)	A (m)	v_{osc} (m/s)	v_r (m/s)	D (m)	f (s^{-1})
1.0	8.69	0.00	0.00	8.69	0.180	
1.5	9.20	0.04	1.72	9.36	0.194	
2.0	9.58	0.09	3.45	10.18	0.211	
2.5	9.88	0.13	5.18	11.16	0.231	
3.0	10.14	0.17	6.92	12.27	0.254	
3.5	10.36	0.21	8.64	13.49	0.279	10.14
4.0	10.56	0.26	10.38	14.80	0.306	
4.5	10.73	0.30	12.10	16.17	0.335	
5.0	10.89	0.34	13.83	17.60	0.365	
5.5	11.04	0.38	15.56	19.08	0.395	
6.0	11.17	0.43	17.29	20.59	0.426	

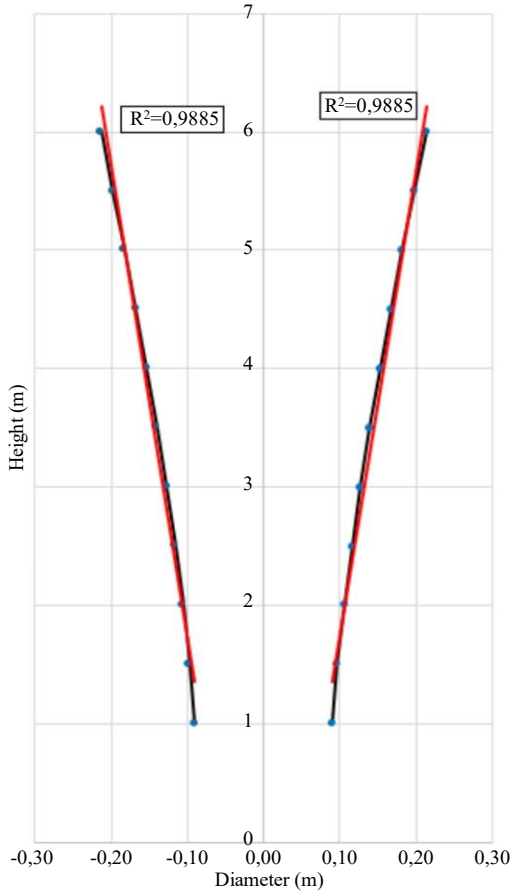

Figure 13. BWT prototype mast design.

Because current industrial tools cannot manufacture a design similar to that shown in Figure 13 (blue line), the practice approximates the curved mast profile to a truncated cone geometry (red line). The high agreement (R^2=0.9885) between the mathematical development and manufacturing approaches validated the proposed method.

CONCLUSIONS

In this study, we propose a mathematical model based on physical laws to describe the mechanical behavior of BWT wind turbines. This behavior corresponds to an oscillation transverse to the incident airflow when the system reaches a high Reynolds number.

Mathematical development results in an algorithm that describes the BWT mast profile under a constant oscillation frequency along the height, to avoid mechanical wear and stress on the mast material. This development shows that the mast geometry is a truncated cone.

Similarly, under the condition of one fixed end and one free-end, a method of describing the bending angle and trajectory of the core is obtained, which allows us to conclude that the height at which the horizontal displacement of the core is negligible is L/2, where L is the height of the core.

The predicted results from the mathematical analysis show good agreement, higher than 95% on average, with reported data in the literature, thus validating the proposed mathematical procedure. A simulation run for a designed prototype shows a high agreement between mathematical development and the linear approach currently adopted by the manufacturing processes (R^2=0.9885); therefore, the proposed methodology for the BWT design is valid.

REFERENCES

1. International Energy Agency. Key World Energy Statistics. Paris: International Energy Agency, 2007. p. 6.
2. International Energy Agency. World Energy Outlook. Paris: OECD/IEA, 2009. p. 17.
3. Kadoshin S, Nishiyama T, Ito T. The trend in current and near-future energy consumption from a statistical perspective. Applied Energy. 2000;67:407–417. DOI: 10.1016/S0306-2619(00)00033-7.
4. Pioro I, Duffey R. Current status of electricity generation in the world and future of nuclear power industry. In: Managing Global Warming. Elsevier; 2019:67–114. DOI: 10.1016/B978-0-12-814104-5.00003-X.
5. Lerede D, Savoldi L. Might future electricity generation suffice to meet the global demand? Energy Strategy Reviews. 2023;47:101080. DOI: 10.1016/j.esr.2023.101080.
6. Armaroli N, Balzani V. The future of energy supply: Challenges and opportunities. Angewandte Chemie. 2007;46:52–66. DOI: 10.1002/anie.200602373, PubMed: 17103469.
7. Breyer C. A global overview of future energy. In: Future Energy. Elsevier; 2020:727–756. DOI: 10.1016/B978-0-08-102886-5.00034-7.
8. Red de política de energía renovable para el Siglo XXI (REN21). Renewables Global Status Report 2023 Collection Energy Demand Modules. Available at: https://www.ren21.net/wp-content/uploads/2019/05/GSR2023-Demand-Launch-Presentation.pdf; 2023.
9. Wolniak R, Skotnicka-Zasadzień B. Development of wind energy in EU countries as an alternative resource to fossil fuels in the years 2016–2022. Resources. 2023;12:96. DOI: 10.3390/resources 12080096.
10. Brown LR. The Great Transition: Shifting from Fossil Fuels to Solar and Wind Energy. WW Norton & Company; 2015.
11. Arutyunov VS, Lisichkin GV. Energy resources of the 21st century: Problems and forecasts. Can renewable energy sources replace fossil fuels? Russian Chemical Reviews. 2017;86:777–804. DOI: 10.1070/RCR4723.
12. Electricity Generation from Solar and Wind Power. Our World in Data. Solar and wind power generation. Ember and Energy Institute. Available from: ourworldindata.org

13. Steg L, Shwom R, Dietz T. What drives energy consumers?: Engaging people in a sustainable energy transition. IEEE Power and Energy Magazine. 2018;16:20–28. DOI: 10.1109/MPE.2017.2762379.
14. Zhao ZY, Chen YL, Chang RD. How to stimulate renewable energy power generation effectively? – China's incentive approaches and lessons. Renewable Energy. 2016;92:147–156. DOI: 10.1016/j.renene.2016.02.001.
15. Sardianou E, Genoudi P. Which factors affect the willingness of consumers to adopt renewable energies? Renewable Energy. 2013;57:1–4. DOI: 10.1016/j.renene.2013.01.031.
16. Yaqoot M, Diwan P, Kandpal TC. Review of barriers to the dissemination of decentralized renewable energy systems. Renewable and Sustainable Energy Reviews. 2016;58:477–490. DOI: 10.1016/j.rser.2015.12.224.
17. Heldeweg MA, Saintier S. Renewable energy communities as 'socio-legal institutions': A normative frame for energy decentralization? Renewable and Sustainable Energy Reviews. 2020;119:109518. DOI: 10.1016/j.rser.2019.109518.
18. Liu J, Zhang D, Cai J, Davenport J. Legal systems, national governance and renewable energy investment: Evidence from around the world. British Journal of Management. 2021;32:579–610. DOI: 10.1111/1467-8551.12377.
19. Wilder M, Drake L. International law and the renewable energy sector. In: Carlarne CP, Gray KR, Tarasofsky R, editors. The Oxford Handbook of International Climate Change Law. UK: Oxford University Press; 2016; pp. 357–90.
20. Mathews J, Thurbon E, Kim SY, Tan H. Gone with the wind: How state power and industrial policy in the offshore wind power sector are blowing away the obstacles to East Asia's green energy transition. Rev Evol Pol Eco. 2023;4:27–48. DOI: 10.1007/s43253-022-00082-7.
21. Markard J, Petersen R. The offshore trend: Structural changes in the wind power sector. Energy Policy. 2009;37:3545–3556. DOI: 10.1016/j.enpol.2009.04.015.
22. Zhixin W, Chuanwen J, Qian A, Chengmin W. The key technology of offshore wind farm and its new development in China. Renewable and Sustainable Energy Reviews. 2009;13:216–222. DOI: 10.1016/j.rser.2007.07.004.
23. Wang L, Wei J, Wang X, Zhang X. The development and prospect of offshore wind power technology in the world. In: World Non-grid-Connected Wind Power and Energy Conference. IEEE; 2009:1–4. DOI: 10.1109/WNWEC.2009.5335761.
24. Da Z, Xiliang Z, Jiankun H, Qimin C. Offshore wind energy development in China: Current status and future perspective. Renewable and Sustainable Energy Reviews. 2011;15:4673–4684. DOI: 10.1016/j.rser.2011.07.084.
25. Linnerud K, Dugstad A, Rygg BJ. Do people prefer offshore to onshore wind energy? The role of ownership and intended use. Renewable and Sustainable Energy Reviews. 2022;168:112732. DOI: 10.1016/j.rser.2022.112732.
26. Xu W, Liu Y, Wu W, Dong Y, Lu W, Liu Y, Zhao B, Li H, Yang R. Proliferation of offshore wind farms in the North Sea and surrounding waters revealed by satellite image time series. Renewable and Sustainable Energy Reviews. 2020;133:110167. DOI: 10.1016/j.rser.2020.110167.
27. Dedecca JG, Hakvoort RA, Ortt JR. Market strategies for offshore wind in Europe: A development and diffusion perspective. Renewable and Sustainable Energy Reviews. 2016;66:286–296. DOI: 10.1016/j.rser.2016.08.007.
28. Kaldellis JK, Kapsali M. Shifting towards offshore wind energy—Recent activity and future development. Energy Policy. 2013;53:136–148. DOI: 10.1016/j.enpol.2012.10.032.
29. Politis ES, Prospathopoulos J, Cabezon D, Hansen KS, Chaviaropoulos PK, Barthelmie RJ. Modeling wake effects in large wind farms in complex terrain: The problem, the methods and the issues. Wind Energy. 2012;15:161–182. DOI: 10.1002/we.481.
30. Barthelmie RJ, Hansen K, Frandsen ST, Rathmann O, Schepers JG, Schlez W, Phillips J, Rados K, Zervos A, Politis ES, Chaviaropoulos PK. Modelling and measuring flow and wind turbine wakes in large wind farms offshore. Wind Energy. 2009;12:431–444. DOI: 10.1002/we.348.

31. Amaral L, Castro R. Offshore wind farm layout optimization regarding wake effects and electrical losses. Eng Appl Artif Intell. 2017;60:26–34. DOI: 10.1016/j.engappai.2017.01.010.
32. Christiansen MB, Hasager CB. Wake effects of large offshore wind farms identified from satellite SAR. Remote Sensing of Environment. 2005;98:251–268. DOI: 10.1016/j.rse.2005.07.009.
33. Sundar RM, Sullivan JP. Performance of wind turbines in a turbulent atmosphere. Solar Energy. 1983;31:567–575. DOI: 10.1016/0038-092X(83)90173-1.
34. Cocina V, Di Leo P, Pastorelli M, Spertino F. Choice of the most suitable wind turbine in the installation site: A case study. In: International Conference on Renewable Energy Research and Applications (ICRERA). IEEE; 2015:1631–1634. DOI: 10.1109/ICRERA.2015.7418682.
35. Armenta-Déu C. Improved marine wind farm layout. Journal of Offshore Structure and Technology. 2024;11:32–40.
36. Guerrero T, Constante J. Distribución factible de aerogeneradores en un parque eólico. OLADE. Available at: https://enerlac.olade.org/index.php/ENERLAC/article/view/22.
37. Tandel R, Shah S, Tripathi S. A state-of-art review on bladeless wind turbine. Journal of Physics: Conference Series. 2021;1950:012058. DOI: 10.1088/1742-6596/1950/1/012058.
38. Vera A, Cardozo N, Jimmikc A. Reynolds number. Available at: https://repository.uniminuto.edu /handle/10656/4849.
39. Manwell JF, McGowan JG, Rogers AL. Wind Energy Explained: Theory, Design and Application. John Wiley & Sons; 2010.
40. Villarreal DJY, S.L., V.B. Resonant Wind Turbines by VIV. Available at: https://vortexblade less.com.
41. Plazaola Iguaran A. Modelización mediante CFD de un campo eólico de aerogeneradores sin palas usando vortex induced vibration (VIV). Repositorio Institucional de Documentos. Available at: https://zaguan.unizar.es/record/120320?ln=es.
42. Sánchez-Hidalgo MÁ, Atienza-Pascual R, Villareal DY. Diseño y Optimización de una Estructura Geométrica Cilíndrica para un Desprendimiento Uniforme de Vórtices de Von Karman. Tecnología y Desarrollo. 2017;15. Repositorio Universidad Alfonso X (UAX), Madrid, Spain.
43. Peterson EW, Hennessey JP Jr. On the use of power laws for estimates of wind power potential. Journal of Applied Meteorology. 1978;17:390–394. DOI: 10.1175/1520-0450(1978)017<0390: OTUOPL>2.0.CO;2.
44. Hsu SA, Meindl EA, Gilhousen DB. Determining the power-law wind-profile exponent under near-neutral stability conditions at sea. Journal of Applied Meteorology. 1994;33:757–765. DOI: 10.1175/1520-0450(1994)033<0757:DTPLWP>2.0.CO;2.
45. Touma JS. Dependence of the wind profile power law on stability for various locations. Journal of the Air Pollution Control Association. 1977;27:863–866. DOI: 10.1080/00022470.1977.10470503.
46. Villarreal DJY. Electrical power generator and an electrical power generation method. US20170284365A1. United States, 2017.

